RSC Advances

ROYAL SOCIETY OF CHEMISTRY

www.rsc.org/advances

RSC Advances

COMMUNICATION

Facile hydrothermal method to prepare graphene quantum dots from graphene oxide with different photoluminescence

Received 00th January 20xx,
Accepted 00th January 20xx

DOI: 10.1039/x0xx00000x

www.rsc.org/

Renbing Tian, Suting Zhong, Juan Wu, Wei Jiang*[a] and Tianhe Wang*[b]

A simple technique to prepare graphene quantum dots (GQDs) by hydrothermal reaction of graphene oxide (GO) sheets with hydrogen peroxide is presented. Complete removal of the hydrogen peroxide after reaction was achieved by catalytic dialysis with manganese oxide. By varying the reaction time, the particle sizes of GQDs could be controlled, leading to variation in photoluminescence. The property of GQDs to produce green and blue photoluminescence was stable. The nanostructure of the prepared GQDs was characterized and discussed in relation to its preparation procedures and behaviors of photoluminescence. The mechanism of the reation was also discussed.

Compared with two-dimensional nanosheets, the zero-dimensional graphene quantum dots (GQDs) not only possess the intrinsic properties of graphene such as large specific surface area, and thermal/chemical stability, but also a number of novel characteristics due to the quantum confinement and edge effects.[1,2] Although there have been numerous methods for preparation of GQDs, they are categorized in either top-down or bottom-up strategies. The top-down methods refer to the cutting of graphene sheets via chemical,[3-5] physical,[23,6] and other techniques.[7,8] Conversely, the bottom-up method involves stepwise synthesis of graphene moieties from organic precursors.[9-11] The hydrothermal method is widely used in the preparation of GQDs from raw materials such as carbon black,[12] carbon fibers,[13] graphene oxide (GO) [21,22] and graphite nanoparticles.[14] Recently, a new technique based on photo-Fenton reaction was proposed.[15] GQDs with uniform lateral dimensions of 40 nm could be obtained from GO in a short time and ambient temperature under a ultraviolet (UV) irradiation (365 nm, 1000 W). However, the conventional hydrothermal methods involve treatments of the raw materials with nitric acid and sulfuric acid followed by a lengthy hydrothermal reaction, which bring about drawbacks of introducing a substantial quantity of acid radicals. Similarly, the solution after photocatalytic treatment by fenton reagents also resulted in large amount of ferric ions as an unwanted by-product. Both of these two methods required lengthy and repeated dialysis process to remove impurity ions because the concentrations of these ions inside and outside the dialysis bag can only reach a dynamic equilibrium. Besides, these techniques only allow GQDs with a single photoluminescence (PL) colour to be produced. Hence, there is a need for a facile, less time consuming and inexpensive method for producing GQDs with multi PL color.

Herein, we report a simple one-step hydrothermal method to produce GQDs via the reaction between hydrogen peroxide and GO in a high temperature and high pressure (HPHT) environment. Hydrogen peroxide was used to generate hydroxyl radicals (·OH) under the HPHT condition as chemical "scissors" to cut down GO sheets. It is worth mentioning that different sizes of GQDs emit various PL are obtained as the reaction proceeds. We can prepare GQDs with green and blue PL via controlling reaction time. The GQDs prepared by this method were excited continuously for 24h under ultraviolet lamp and showed no visible PL decay, the excellent stability implying potential applications in drug delivery and cellular imaging. The technique established in this work uses only common laboratory reagents and a Teflon-lined stainless-steel autoclave to provide HPHT conditions. The excessive hydrogen peroxide is conveniently eliminated via a simple and continuous catalytic decomposition. Therefore the method has apparent advantages over other GQDs-making techniques and may reduce the cost of mass production significantly.

·OH is a powerful oxidizing reagent with a standard electrode potential of 2.8V.[16] A possible mechanism of cutting GO by ·OH was described previously.[15] The carbon atoms connected with the hydroxyl and epoxide are attacked by ·OH to break the C-C or C=C bonds, and then, the newly formed oxygen-containing groups serve as new reaction sites. The reaction mechanism between ·OH and hydroxyl/epoxide was discussed by Bai *et al.*[24] and Zhou *et al.*[15] in detail. Take hydroxyl as a sample, a possible mechanism is shown in Figure S1(a), this process was repeated in whole reaction, and ·OH acted as the scissor to break C-C bond (Figure S1b). In fact, XPS results of GO, GQDs1 and GQDs2 also prove this mechanism. As shown in Figure S2, four peaks of C 1s at 284.9, 286.9, 288.1 and

[a]*National Special Superfine Powder Engineering Research Center, Nanjing University of Science and Technology, 210094, Nanjing, China. E-mail: superfine_jw@126.com*
[b]*Nanjing University of Science and Technology, 210094, Nanjing, China. E-mail: thwang56@126.com*

289.4 eV correspond to C=C, C-O, C=O and O-C=O respectively. Obviously, the intensity of C-O decreased as reaction preceded, which means hydroxyl and epoxide groups decreased gradually. Ultimately, large GO sheets are cut into small fragments. Hydrogen peroxide cleaves at high temperature to form ·OH with the activation energy of 48.5 kcal.[17] According to the Arrhenius equation, it is easier to form ·OH at higher the temperature. Therefore, the high temperature condition provided by autoclave is thermodynamically favorable for the reaction between ·OH and GO sheets. On the other hand, at elevated temperature, hydrogen peroxide tends to decompose into oxygen. However the pressure inside the autoclave at 170℃ would be high, which would restrict the decomposition of hydrogen peroxide and help to maintain sufficient source of ·OH. Therefore it is concluded that the HPHT condition created by autoclave is favorable to the H_2O_2/GO reaction both thermodynamically and kinetically.

GQDs were successfully prepared through the hydrothermal cutting method. The experiment section is discussed in supplementary information in detail. Homolysis of hydrogen peroxide was used to produce hydroxyl radicals as "scissors" to break down GO sheets. Two samples (GQDs1 and GQDs2) were prepared under identical hydrothermal conditions (170℃) but with different reaction times, 60 and 80 min, respectively. The product yield is 32% and 57% for GQDs1 and GQDs2. Part of the product after 60 min of hydrothermal treatment was larger than 200 nm, which was removed in filter process via 0.22-μm membrane. So the product yield of GQDs1 was lower than GQDs2. Quinine sulfate was chosen as a standard for calculating quantum yield (QY), which was 3.6% and 5.3%, respectively (Table S1). In Figure 1a, GQDs1 and GQDs2 solutions after hydrothermal reaction without further treatment are shown. Figure 1b shows GQDs1 and GQDs2 solutions after filtration through a 0.22-μm membrane and dialysis treatment. It is interesting to notice that as the hydrothermal reaction proceeded, the brownish colour faded gradually, eventually became colourless. A group of photographic shows the colours and the PL properties of solution with the reaction time increased. As shown in Figure S3, the solution colour turned from brown to yellow and colourless with the reaction time increased from 60 min to 70 min and 80 min. Meanwhile, the PL of solution show green, green and blue when the reaction time is 60 min, 70 min and 80 min. Besides, if the reaction time was extended to 4 h, PL of the product solution disappeared. In addition, no GQDs can be found in AFM image (as shown in Figure S4). After long time of hydrothermal treatment, GO sheet was decomposed into small inorganic molecular.

Figure 2 shows UV-vis absorption spectra of GQDs hydrothermal treated for 60, 80 min and GO sheets, respectively. An apparent blue shift from 230 to 225 nm is observed when GO sheets are cut into GQDs, suggesting a higher energy gap in GQDs. This is consistent with the quantum confinement effect.[18] In UV-vis spectra, two peaks can be observed. The peak of 225 nm due to the π-π* transition of aromatic C=C bond and the shoulder at 300 nm assigned to the n-π* transition of C=O bond.[28] For the former, π-electron motion in delocalized π bond composed by sp^2 carbons. Under strong oxidation environment, previous sp^2 clusters were destroyed which influence the size of sp^2 clusters further. The energy gap of π-π* transition depends on the size of sp^2 clusters or conjugation length.[29] However, for C=O bond, with the size decrease of graphene oxide, the environment of electron movement didn't change a little. Therefore, there are 5 nm of blue shift in π-π* transition, and no obvious blue shift in n-π* transition.

Raman spectroscopy was also employed to characterize the GQDs. The results indicate a G band of ordered sp^2 bonded carbon and a D band of disordered carbon, respectively. As shown in Figure 3d, a clear red shift is observed from 1590 cm^{-1} to 1620 cm^{-1} for GQDs. The intensities of D to G (I_D/I_G) have no apparent differences between GO sheets and GQDs.

Transmission electron microscopy (TEM) images (Figure. 3) show that the GQDs2 had an average lateral dimension, of ~60 nm. There are some large graphene sheets (with a size range between 50 and 200 nm) in GQDs1, as shown in the inset of picture 3(a). This result indicates that as the reaction time prolonged from 60 min to 80 min, the average size of GQDs were further reduced significantly. It is likely that this reduction of GQDs size caused the blue shift of PL, as shown in Figure 2. The crystalline structure and electron diffraction pattern was observed in the high resolution transmission electron microscopy (HRTEM) images with a fringe lattice spacing of ~ 0.252 and 0.249 nm, respectively, matching well with the data of graphite (0.246 nm) within the limit of error.[19] Atomic force microscope (AFM) images with a scanning scope of 5x5 μm is shown in Figure 4. Clearly, some larger graphene sheets (sized 50~200 nm) still existed in GQDs1 (Figure 4a). This had inevitably affected properties of the solution colour and PL for GQDs1. The thickness for both GQDs was between 0.5 and 1.5 nm, corresponding to 1-3 graphene layers.

The PL properties of GQDs are shown in Figure 5, the GQDs with synthesized time of 60 and 80 minutes display green and blue emission colours at the excitation wavelength of 365 nm, respectively (Figure 2). For GQDs1, when the excitation wavelength changes from 330 to 370 nm, the PL peak shifts from 450 to 510 nm, and the PL intensity alters correspondingly. GQDs2 share the same tendency. The excitation dependent properties of GQDs were also observed with other luminescent carbon nanomaterials.[15] This may be interpreted by that GQDs have different emissive sites and different sizes.[12] As shown in Figure 5c, the PL excitation (PLE) spectra were measured at the detection emission wavelength of 450 nm, both samples have a maximum PLE intensity at 340 nm. It is interesting to find that the fluorescence intensity curve is fairly smooth when the solution is colourless, because there is a small amount of large GO sheets (but smaller than 0.22 μm) in the yellow solution (Figure 1) and this affected the shape of intensity curve (Figure 5a). A detailed discussion of relationship between low impurities, PL spectra, and quantum yield is presented in supplementary information. The PL lifetimes curve was recorded for the GQDs transitions at 460 nm emission and 340 nm excitation by a transient fluorescence spectrometer. Both GQDs1 and GQDs2 were well fitted to a bitangent exponential function as shown in Figure S5 and Figure S6. Besides, the instrument response function and decay curve of GQDs1 and GQDs2 are also listed in black and red colour. For GQDs1, the observed lifetimes are t_1 = 1.34 ns and t_2 = 9.85 ns while lifetimes are t_1 = 1.81 ns and t_2 = 10.31 ns for GQDs2. The lifetime in nanosecond means the GQDs are suitable for biological, optoelectronic and other applications. The existing explanations of PL mechanism include defect state emission and intrinsic state emission caused by zigzag sites or electron-hole recombination.[25] Wen *et al.* proposed that two spectral overlapped

intrinsic (core) and extrinsic (surface) PL bands of carbon quantum dots and GQDs are responsible for the PL mechanism and excitation wavelength dependent PL.[30] Zhu *et al.* used the defect state emission to explain the PL mechanism, which is related with the presence of oxygenous functional groups on the surface of GQDs.[26] According to XPS results (Figure S2) and UV-vis (Figure 2) spectra, there is a quantity of oxygen-containing groups on GQDs. So it can be inferred that the PL mechanism could be explained by defect states caused by oxygen-containing groups located on the plane of GQDs.[27] The excitation wavelength dependent PL properties are also caused by the surface oxygen-containing functional groups which have different energy levels,[12] as shown in Figure S7. The UV-vis absorption peaks at 225 nm (5.51 eV) and 300 nm (4.14 eV) correspond to electron transitions of π-π* of C=C and n-π* of the C=O bond respectively.

A tentative mechanism is proposed here to interpret the different PL as observed with GQDs1 and GQDs2. As depicted in Figure 6, ·OH cut the GO sheets into small fragment as the hydrothermal reaction proceeded. The larger average size of GQDs1 resulted in a red shift in its PL as compared with that for GQDs2. This red shift in PL wavelength for GQDs1 was caused by the moderately larger particle sizes, and in principle, this is consistent with the quantum size theory. [20]

We have presented a simple but novel method to prepare GQDs by hydrothermal treatment of GO sheets with hydrogen peroxide and the technique to purify them by a manganese dioxide catalyzed dialysis process. The facile method shows prominent advantages of one-step reaction, low time-consumption, continuous removal of the hydrogen peroxide and perhaps the most interesting of all, the controllable size of GQDs leading to variation in PL. The nanostructure of the prepared GQDs were characterized and discussed in relation to its preparation and behaviors of PL. By varying reaction time, GQDs exhibiting stable green and blue PL were produced. These features make it a competitive candidate for applications in biomedical fields.

This work was supported by a Project Funded by the Priority Academic Program Development of Jiangsu Higher Education Institutions.

Notes and references

1 C. O. Girit, J. C. Meyer, R. Erni, M. D. Rossell, C. Kisielowski, L. Yang, C. H. Park, M. F. Crommie, M. L. Cohen, S. G. Louie and Zetti, *Science*, 2009, **323**, 1705–1708.
2 L. A. Ponomarenko, F. Schedin, M. I. Katsnelson, R. Yang, E. W. Hill, K. S. Novoselov and A. K. Geim, *Science*, 2008, **320**, 356–358.
3 D. Y. Pan, J. C. Zhang, Z. Li and M. H. Wu, *Adv. Mater.*, 2010, **22**, 734–738.
4 S. J. Zhu, J. H. Zhang, C. Y. Qiao, S. J. Tang, Y. F. Li, W. J. Yuan, B. Li, L. Tian, F. Liu, R. Hu, H. N. Gao, H. T. Wei, H. Zhang, H. C. Sun and B. Yang, *Chem. Commun.*, 2011, **47**, 6858–6860.
5 F. C. Liu, T. Tang, Q. Feng, M. Li, Y. Liu, N. J. Tang, W. Zhong and Y. W. Du, *J. Appl. Phys.*, 2014, **115**, 164307.
6 X. Sun, Z. Liu, K. Welsher, J. T. Robinson, A. Goodwin, S. Zaric and H. Dai, *Nano Res.*, 2008, **1**, 203–212.
7 J. Güttinger, C. Stampfer, T. Frey, T. Ihn and K. Ensslin, *Phys. Status Solidi B*, 2009, **246**, 2553-2557.
8 M. Zhang, L. L. Bai, W. H. Shang, W. J. Xie, H. Ma, Y. Y. Fu, D. C. Fang, H. Sun, L. Z. Fan, M. Han, C. M. Liu and S. H. Yang, *J. Mater. Chem.*, 2012, **22**, 7461–7467.
9 X. Yan, B. Li, X. Cui, Q. Wei, K. Tajima and L. S. Li, *J. Phys. Chem. Lett.*, 2011, **2**, 1119–1124.
10 Y. Q. Dong, J. W. Shao, C. Q. Chen, H. Li, R. X. Wang, Y. W. Chi, X. M. Lin and G. N. Chen, *Carbon*, 2012, **50**, 4738–4743.
11 L. B. Tang, R. B. Ji, X. K. Cao, J. Y. Lin, H. X. Jiang, X. M. Li, K. S. Teng, C. M. Luk, S. J. Zeng, J. H. Hao and S. P. Lau, *ACS Nano*, 2012, **6**, 5102–5110.
12 Y. Q. Dong, C. Q. Chen, X. T. Zheng, L. L. Gao, Z. M. Cui, H. B. Yang, C. X. Guo, Y. W. Chi and C. M. Li, *J. Mater. Chem.*, 2012, **22**, 8764-8766.
13 J. Peng, W. Gao, B. K. Gupta, Z. Liu, R. R. Aburto, L. H. Ge, L. Song, L. B. Alemany, X. B. Zhan, G. H. Gao, S. A. Vithayathil, B. A. Kaipparettu, A. A. Marti, T. Hayashi, J. J. Zhu and P. M. Ajayan, *Nano Lett.*, 2012, **12**, 844−849.
14 F. Liu, M. H. Jang, H. D. Ha, J. H. Kim, Y. H. Cho and T. S. Seo, *Adv. Mater.*, 2013, **25**, 3657–3662.
15 X. J. Zhou, Y. Zhang, C. Wang, X. C. Wu, Y. Q. Yang, B. Zheng, H. X. Wu, S. W. Guo and J. Y. Zhang, *ACS nano*, 2012, **6**, 6592-6599.
16 K. Ikehata, M. G. El-Din, *Environ. Eng. Sci.*, 2006, **5**, 81–135.
17 D. C. Conway, *J. Phys. Chem.*, 1957, **61**, 1579–1580.
18 K. Sung, S. W. Hwang, M. K. Kim, D. Y. Shin, D. H. Shin, C. O. Kim, S. B. Yang, J. H. Park, E. Hwang, S. H. Choi, G. Ko, S. Y. Sim, C. Sone, H. J. Choi, S. K. Bae and B. H. Hong, *ACS nano*, 2012, **6**, 8203–8208.
19 Y. Baskin and L. Meyer, *Phys. Rev.*, 1955, **100**, 544.
20 C. X. Xia and S. Y. Wei, *Microelectron. J.*, 2006, **37**, 1408–1411.
21 M. Li, W. B. Wu, W. C. Ren, H. M. Cheng, N. J. Tang, W. Zhong and Y. W. Du, *Appl. Phys. Lett.*, 2012, **101**, 103107.
22 Q. Feng, Q. Q. Cao, M. Li, F. C. Liu, N. J. Tang and Y. W. Du, *Appl. Phys. Lett.*, 2013, **103**, 013111.
23 S. Zhuo, M. Shao and S. T. Lee, *ACS Nano*, 2012, **6**, 1059–1064.
24 H. Bai, W. T. Jiang, G. P. Kotchey, W. A. Saidi, B. J. Bythell, J. M. Jarvis, A. G. Marshall, A. S. Robinson and A. Star, *J. Phys. Chem. C*, 2014, **118**, 10519-10529.
25 S. J. Zhu, J. H. Zhang, S. J. Tang, C. Y. Qiao, L. Wang, H. Y. Wang, X. Liu, B. Li, Y. F. Li, W. L. Yu, X. F. Wang, H. C. Sun and B. Yang, *Adv. Funct. Mater.*, 2012, **22**, 4732– 4740.
26 Z. C. Huang, Y. T. Shen, Y. Li, W. J. Zheng, Y. J. Xue, C. Q. Qin, B. Zhang, J. X. Hao and W. Feng, *Nanoscale*, 2014, **6**, 13043-13052.
27 L. Tang, R. Ji, X. Li, K. S. Teng and S. P. Lau, *Part. Part. Syst. Char.*, 2013, **30**, 523–531.
28 S. H. Song, M. H. Jang, J. Chung, S. H. Jin, B. H. Kim, S. H. Hur, S. Yoo, Y. H. Cho and S. Jeon, *Adv. Optical Mater.*, 2014, **2**, 1016-1023.
29 G. Eda, Y. Y. Yue, C. Mattevi, H. Hamaguchi, H. A. Chen, I. S. Chen, C.W. Chen and M. Chhowalla, *Adv. Mater.*, 2010, **22**, 505-509.
30 X. M. Wen, P. Yu, Y. R. Toh, X. T. Hao and J. Tang, *Adv. Optical Mater.*, 2013, **1**, 173-178.

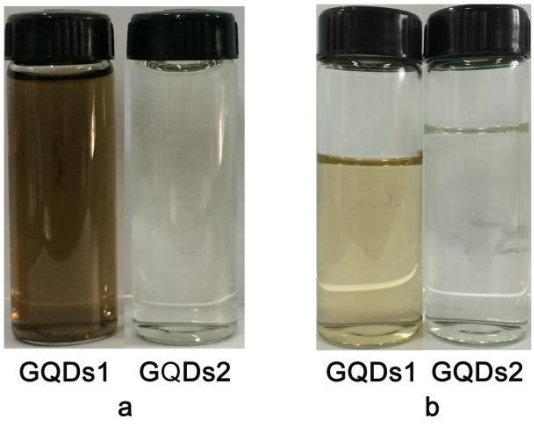

Fig. 1 (a) Solutions after hydrothermal reaction without further treatment and (b) solutions after filtration and dialysis treatment.

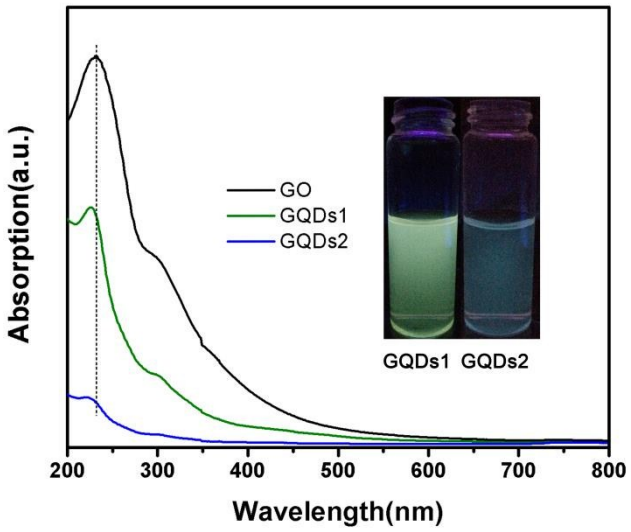

Fig. 2 UV-vis absorption of GO, GQDs1 and GQDs2 in water solution. Inset: optical photograph of GQD solutions under UV light with 365 nm excitation.

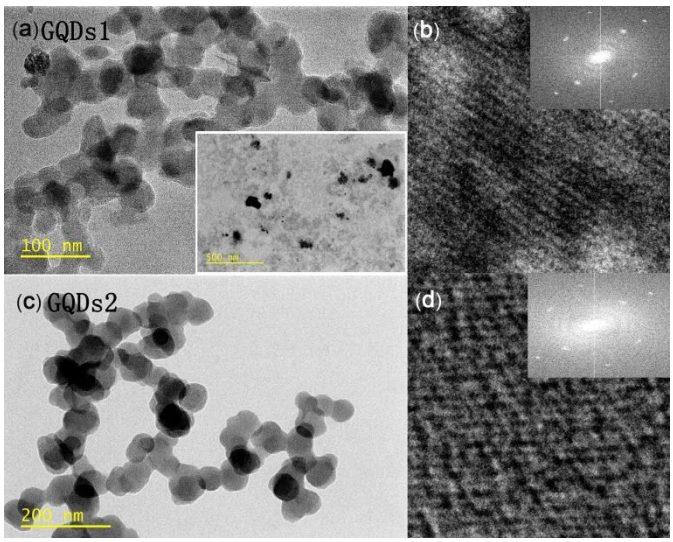

Fig. 3 TEM images of the as-generated GQDs1 (a) and GQDs2 (c), respectively. Inset in picture (a) shows some large GO sheets in GQDs1 with scale bar of 500 nm. HRTEM images of GQDs1 (b) and GQDs2 (d) shows the lattice fringes and electron diffraction pattern of GQDs in the inset.

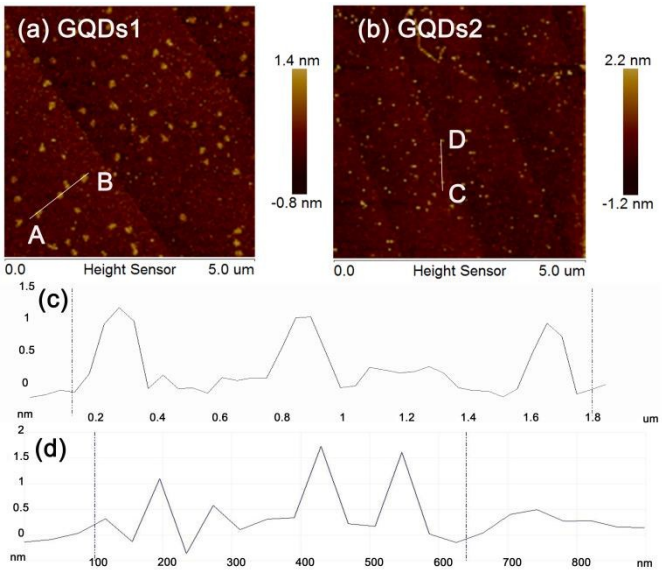

Fig. 4 the AFM images of GQDs1 (a) and GQDs2 (b) with a scanning scope of 5x5 μm. Picture (c) and (d) are the height profile along the line from A to B and C to D, respectively.

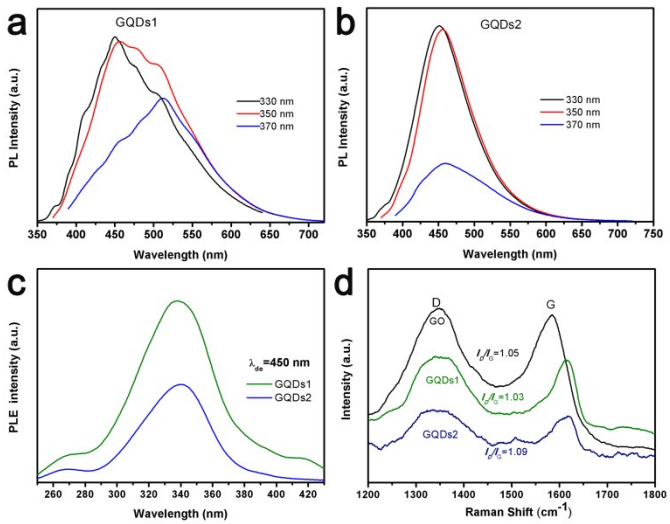

Fig. 5 (a) PL spectra of the GQDs1 at different excitation wavelengths. (b) PL spectra of GQDs2 at different excitation wavelengths. (c) PLE spectra with the detection wavelength of 450 nm. (d) Raman spectra of GO, GQDs1 and GQDs2.

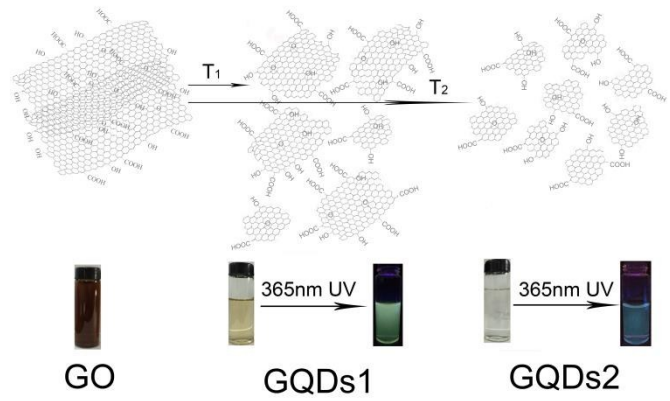

Fig. 6 Schematic representation of mechanism for the reaction and different PL. T_1 is 60 min and T_2 refers to 80 min.

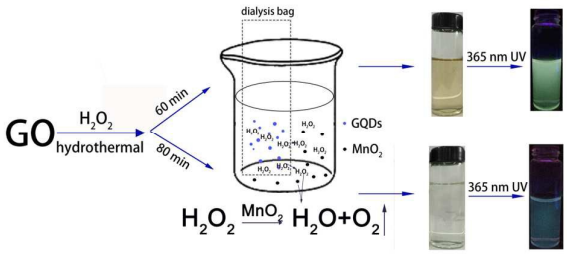

GQDs exhibiting multi-colour photoluminescence were prepared by reacting GO with H_2O_2 and a novel purify method was proposed.